NIPPON STEEL TECHNICAL REPORT No. 58 JULY 1993

UDC669.14.018.292-413 : 621.791.72

Development of Heavy Steel Plates with Excellent Electron Beam Weldability

Takashi Inoue*1 Koji Tanabe*1
Masahiro Ohara*1 Kunio Koyama*1
Yukio Tomita*1 Rikio Chijiiwa*1
Yukio Tsuda*2 Seiji Isoda*3

Abstract:

Electron beam welding is expected to enhance the welding efficiency of heavy steel plates. The electron beam weldability of heavy steel plates was studied, and the following findings were obtained. The toughness of electron beam welded joints of conventional steel plates was investigated. Electron beam welded joints of 490-MPa and 590-MPa steels, each with a coarse upper bainite microstructure, were found to be low in toughness. The low-toughness region was successfully arranged by the carbon content and the ideal critical diameter of hardenability. Lowering the aluminum content was found to improve the toughness of electron beam welds in the 490-MPa steel. On the basis of this finding, a low aluminum-titanium oxide-treated steel, designated SGV480, was developed. Reducing the phosphorus content to an extremely low level was found to improve the solidification segregation and toughness of electron beam welds in the 590-MPa steel. This study result led to the development of an ultralow-phosphorus, low-nitrogen, and low-carbon steel designated SQV2B.

1. Introduction

Welding of heavy steel plates used to fabricate pressure vessels and reactor vessels requires many passes and high-temperature preheating. Electron beam welding (EBW) permits deep-penetration, single-pass welding as shown in **Photo 1**. It improves in efficiency with increasing plate thickness as compared with conventional welding processes such as submerged arc welding (SAW), as shown in **Fig. 1**[1,2]. The absence of a hydrogen source

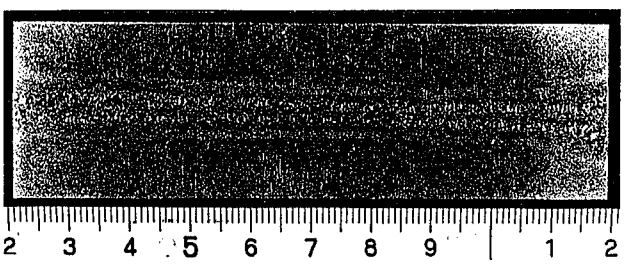

Photo 1 Example of cross section through electron beam weld

*1 Technical Development Bureau
*2 Nagoya Works
*3 Kimitsu Works

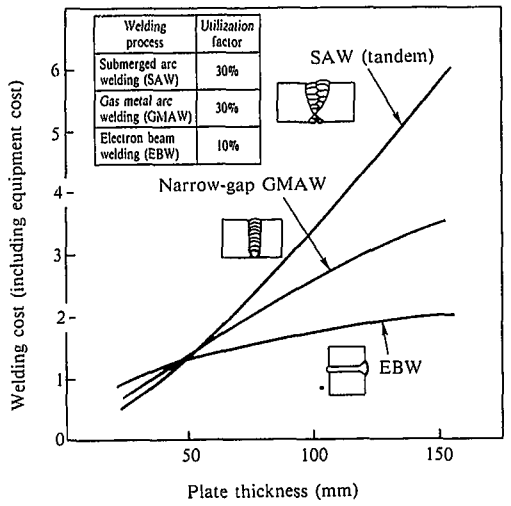

Fig. 1 Effect of plate thickness on welding cost for various welding processes[1]

in EBW reduces the possibility of cold cracking in normal plate welds[3]. Further, blowhole and other defect considerations once imposed restrictions upon the gas composition of steel to be electron beam (EB) welded. However, beam oscillation and other advanced EBW techniques have reduced the gas volume[4] so that it is no longer a problem in normal steel plates[5]. Steel is said to be unsusceptible to hot cracking if the carbon content is less than 0.35% and the combined phosphorus and sulfur content is less than 0.03%[6]. These carbon, phosphorus, and sulfur requirements can be met by heavy steel plates in current use.

These results suggest the applicability of EBW to various structures. EB welded joint performance has been studied for some of the conventional steels[5,7] and for carbon-manganese steels[8], but not systematically as yet. Generally, weld metal (WM) is a cast structure, which varies with steel production conditions, heating temperature, and cooling rate. The composition of welding material is designed to meet these conditions. Since EBW uses no welding materials, the composition of the weld metal is the same as that of the base plate steel. This leaves concern about a loss in toughness.

This report pursues problems with the toughness of EB welds in conventional steel plates for pressure vessels and similar applications, centering on Charpy impact test results, and describes the ensuing development of new electron beam weldable steels with improved weld-metal toughness.

2. Properties of Electron Beam Welded Joints of Conventional Steels

To clarify problems with the application of EBW, conventional heavy steel plates were electron beam welded, and the resulting joints were investigated for toughness in the as-welded condition and after post-weld heat treatment (PWHT).

2.1 Test steels

The chemical compositions of the test steels are as listed in **Table 1**. Each is a steel in current use. Steel A is a mild steel, steel B is a 490-MPa low-carbon, high-copper and high-nickel steel, and steel C is a 490-MPa low-copper, low-nickel and low-vanadium steel. The last two steels are manufactured by the thermomechanical control process (TMCP). Steel D is a 590-MPa steel, steel F is a 780-MPa steel, steel G is a 1.25% Cr-0.5% Mo steel, and steel H is a 2.25% Cr-1% Mo steel.

2.2 EBW and PWHT conditions

The toughness of EB weld is governed by the chemical composition and cooling rate. The cooling rate of the fusion line (FL) of EB weld depends on the beam width as shown in **Fig. 2**. The cooling time from 800 to 500°C is given by the equation shown in **Fig. 2**[9]. The two sets of welding conditions in **Table 2** were

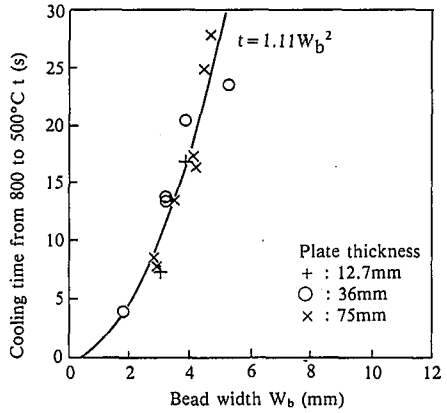

Fig. 2 Relation between bead width and cooling time from 800 to 500°C[9]

Table 2 *Test EBW conditions*

Condition set	Acceleration voltage (kV)	Beam current (mA)	Speed (mm/min)	Beam oscillation		Target bead width (mm)	Cooling time* 800-500 (s)
				Pattern	Width (mm)		
A	150	200	300	No		2.6	7.5
B	150	230	300	Oval	2.0	4.6	23.5

*Calculated by equation shown in Fig. 2.

Table 1 Test steels (conventional steels)

Symbol	Steel	Chemical composition (%)												$Ceq_{(WES)}$* (%)
		C	Si	Mn	P	S	Ni	Cu	Cr	Mo	V	Nb	B	
A	SM400	0.13	0.24	1.01	0.022	0.006	—	—	—	—	—	—	—	0.31
B	490 MPa	0.09	0.27	1.25	0.004	0.001	0.73	0.32	—	—	—	0.01	—	0.33
C	490 MPa	0.11	0.35	1.46	0.025	0.004	0.14	0.14	—	—	0.04	0.03	—	0.38
D	590 MPa	0.14	0.31	1.12	0.007	0.002	0.36	0.31	0.18	—	0.04	0.02	—	0.40
F	780 MPa	0.12	0.24	0.86	0.014	0.004	0.90	0.21	0.44	0.41	0.04	—	0.0009	0.49
G	1.25Cr-0.5Mo	0.13	0.48	0.60	0.006	0.003	0.18	—	1.42	0.63	—	—	—	0.70
H	2.25Cr-1Mo	0.12	0.19	0.58	0.005	0.004	—	—	2.37	1.08	—	—	—	0.97

*$Ceq_{(WES)} = C + Si/24 + Mn/6 + Ni/40 + Cr/5 + Mo/4 + V/14$

thus used as test EBW conditions.

The PWHT conditions were 690°C and 1 h for the chromium-molybdenum steels and 620°C and 1 h for the other steels.

2.3 EB welded joint Charpy impact test results and discussion

Fig. 3 shows the Charpy impact test results of EB welded joints of steels in the as-welded condition when the bead width is 4.6 mm. Under this condition as shown, the toughness of EB welds is low in the 490-MPa steels and the 590-MPa steel, but high in the 780-MPa steel and the Cr-Mo steels. The fusion line exhibited higher Charpy impact toughness than the weld metal.

The Charpy impact fracture path tended to deviate toward the base metal side in the high-toughness region, but not when toughness was less than 70 J. From this fact the transition temperature at which the absorbed energy becomes 70 J is correlated with the carbon equivalent (Ceq) of the steels, as shown in **Fig. 4**. The Charpy impact toughness was the lowest for the 490-MPa steels with a coarse upper bainite (Bu) microstructure. Each steel exhibited higher toughness when the bead width was 2.6 mm than when it was 4.6 mm. This may be attributed to the microstructural change described later and kinematic factors[7,10].

The change in toughness with PWHT is summarized by the same index for the steels in **Fig. 5**. All steels except the 780-MPa steel improved toughness. Temper embrittlement is blamed for the 780-MPa steel that has high hardenability[11].

3. Effects of Carbon Content and Ideal Critical Diameter (Di) on Toughness of Electron Beam Welds in 490-MPa Steels

Alloying elements were studied for their effect on the toughness of EB welds in the 490-MPa steels.

3.1 Test method

Test steels had the ideal critical diameter (Di) changed by varying the carbon content from 0.05 to 0.20% and varying the contents of such alloying elements as manganese, molybdenum, chromium, nickel, copper and boron against each carbon content. Another steel series had niobium, vanadium, and other precipitation hardening elements added. These two series of steel were melted in a small heat size, rolled to 50-mm thick plates, and quenched and tempered (QT).

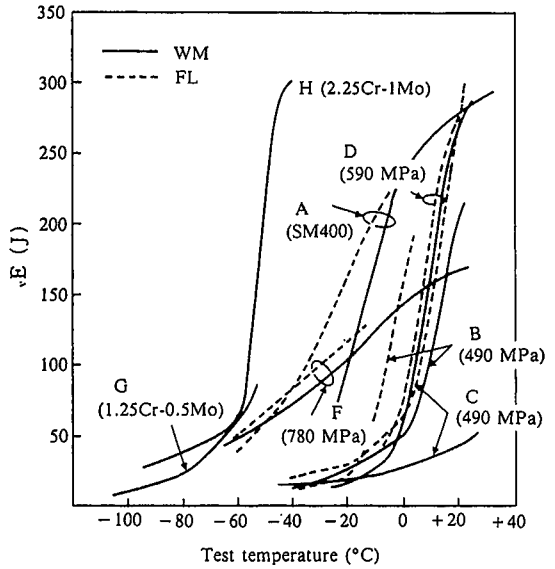

Fig. 3 Charpy impact test results of conventional steels (bead width 4.6 mm, 1/2t)

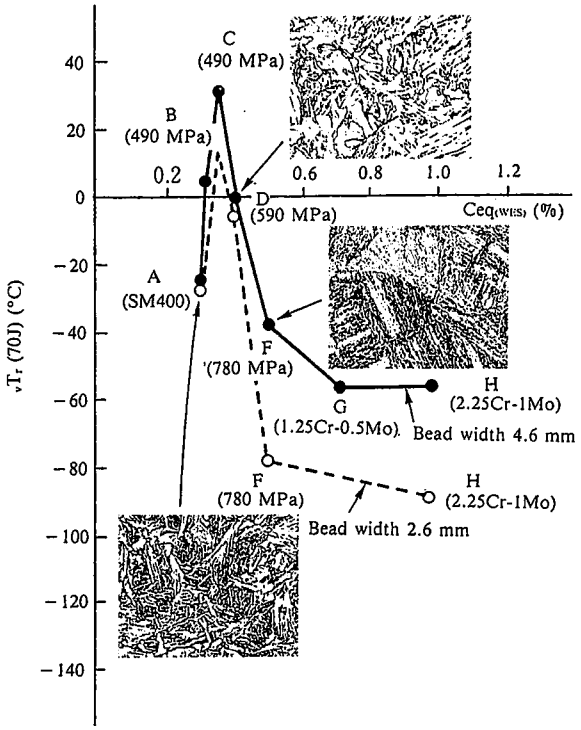

Fig. 4 Relation between Ceq and $_vT_r$ (70 J) (as welded, weld metal)

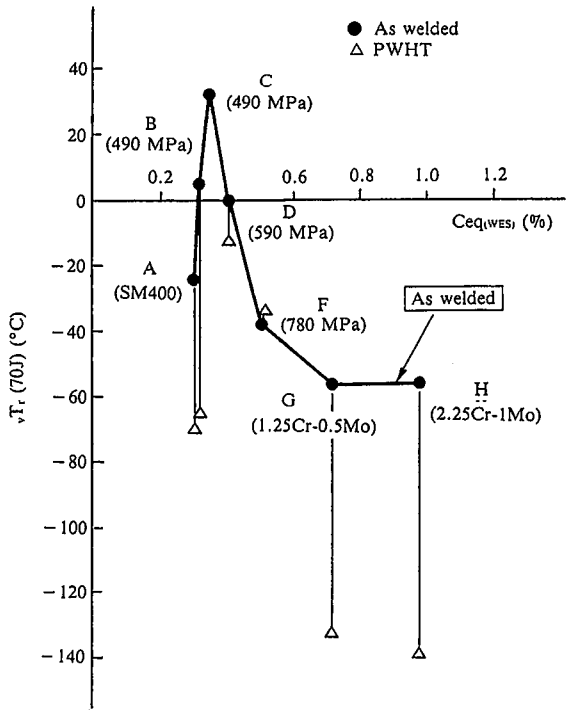

Fig. 5 Relation between Ceq and $_vT_r$ (70 J) after stress relieving (bead width 4.6 mm)

EBW conditions were based on the bead width of 4.6 mm as already presented.

3.2 Test results

Fig. 6 shows the effects of carbon content and the ideal criti-

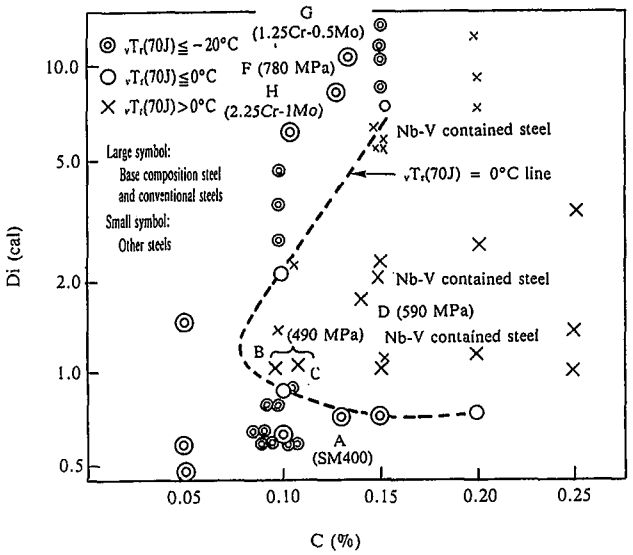

Fig. 6 Relation between carbon content and ideal critical diameter Di on $_vT_r$ (70 J) (bead width 4.6 mm, as welded)

cal diameter Di as arranged by $_vT_r$ (70 J) in the same way as in Chapter 2. The $_vT_r$ (70 J) = 0°C line is a C curve. Inside of the C curve, the microstructure is coarse upper bainite, and $_vT_r$ (70 J) is in the range above 0°C. When the bead width was greater, the C curve somewhat shifted toward the lefthand side, but indicated the same tendency[12]. The base composition referred to here has only the carbon, manganese, and molybdenum contents varied. PWHT improved toughness at the low end of the Di range, but when precipitation hardening elements were present, there were cases of precipitation embrittlement causing a loss in toughness.

4. Development of Carbon Steel SGV480 for Pressure Vessels

As described in Chapter 3, the chemical composition of the steel for EBW can be designed as falling outside of the C curve. For example, it would be satisfactory if the same strength can be obtained by decreasing the carbon content and increasing the ideal critical diameter Di. Specified composition limitations, however, make it difficult to apply these methods to the carbon steel SGV480 for pressure vessels described in this chapter and the quenched and tempered manganese-molybdenum-nickel steel SQV2B for pressure vessels described in the next chapter. Therefore, other methods must be employed to improve the toughness of EB welds in these steels. This chapter describes the toughness improvement of EB welds in the 490-MPa steels of small ideal critical diameter Di.

4.1 Microstructure grain size refinement by oxygen enrichment

According to the findings obtained for arc welding[13], a study was made of the method of refining the microstructure by increasing the oxygen content[14].

4.1.1 Test method

Electron beam welding was conducted using gas metal arc weld (GMAW) metals of the chemical compositions shown in **Table 3**. The weld metal GMAW-1 containing titanium and the weld metal GMAW-2 containing no titanium were applied. To investigate the effect of aluminum, aluminum powder was added during EBW in some test runs.

Table 3 Chemical compositions of GMAW metals

Symbol	Chemical composition (wt%)						(ppm)	
	C	Si	Mn	Cu	Ti	Al	O	N
GMAW-1	0.10	0.68	1.36	0.16	0.02	0.005	490	87
GMAW-2	0.08	0.63	1.33	0.20	<0.002	0.006	500	115

4.1.2 Test results and discussion

The oxygen content dropped to about 130 ppm, but a microstructure predominantly composed of acicular ferrite (AF) was obtained, irrespective of whether or not titanium was contained. Nonmetallic inclusions that served as ferrite transformation nuclei were analyzed by energy-dispersive X-ray spectroscopy (EDX). From these results, composite oxides of the Al-Si-Mn-Ti composition system were detected when titanium was contained, and composite oxides of the Al-Si-Mn composition system were detected when titanium was not contained. The addition of 0.04% aluminum produced a lath-like microstructure for either weld metal.

The above results indicated that EBW can produce acicular ferrite as produced by arc welding if the aluminum-oxygen balance remains good and that titanium oxides are not a necessity as ferrite transformation nuclei. The aluminum-oxygen balance is arranged by the relation shown in **Fig. 7** according to the findings obtained from arc welding. When the aluminum content is high, acicular ferrite is not obtained unless the oxygen content is also high[15]. Increasing the oxygen content is expected to improve the toughness of EB welds. A higher oxygen content, however, leads to the occurrence of weld defects as noted in Chapter 1. Therefore, microstructure grain refinement at a low oxygen content is the only practical method.

4.2 Study of microstructure grain refinement at low oxygen content levels

A low aluminum content is considered necessary at a low oxygen content. When the effective utilization of oxides is taken into account, there should be a lower limit to the necessary oxygen content, but no definite values are available in this respect.

4.2.1 Test method

As shown in **Table 4**, two steels, J and K, were melted in a small heat size by setting the oxygen content at the same level as the conventional steels for pressure vessels and by changing the aluminum content, and were rolled to 12.7-mm thick plates. The plates were then electron beam welded to a bead width of

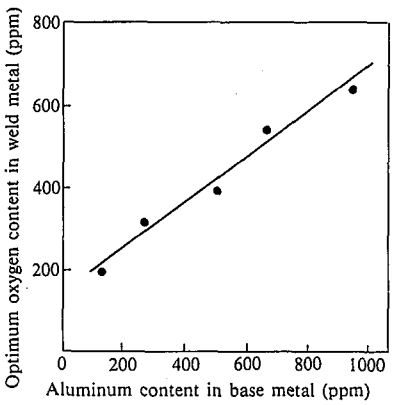

Fig. 7 Relationship between aluminum content and optimum oxygen content[15]

Table 4 Chemical compositions of steels melted in small heat size to investigate effect of aluminum content

(wt%, *ppm)

Symbol	C	Si	Mn	P	S	Al	N*	O*
J	0.10	0.26	1.45	<0.005	0.006	0.027	43	27
K	0.10	0.26	1.45	<0.005	0.007	<0.002	43	26

4 mm.

4.2.2 Test results

The microstructures of EB weld metals in the steels J and K are comparatively shown in **Photo 2**. As already noted in Chapter 2, the microstructure was composed mainly of upper bainite for the steel J containing 0.027 wt% aluminum, and of fine acicular ferrite for the steel K with a lower aluminum content. The oxygen content was less than 10 ppm in the weld metal of each EB weld. **Fig. 8** shows the results of EDX analysis of nonmetallic inclusions considered to serve as ferrite transformation nuclei when no aluminum is contained. MnS inclusions having Al-Si-Mn composite oxides as nuclei were identified[16-18].

4.3 Development of low-aluminum and low-titanium oxide-treated steel SGV480

It was found possible to improve the weld-metal toughness of EB welds by lowering the aluminum content. With actual welded joints, it is also necessary to improve the toughness of the heat-affected zone (HAZ). A titanium oxide-treated steel with an essentially low aluminum content and excellent HAZ toughness was studied[19].

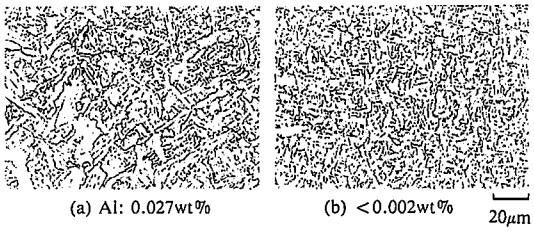

Photo 2 Effect of aluminum content on microstructure of EB weld metal

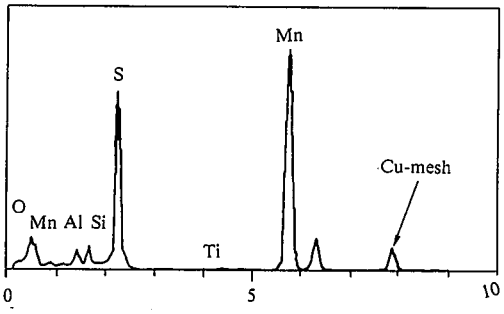

(a) Spectrum from center of nonmetallic inclusions

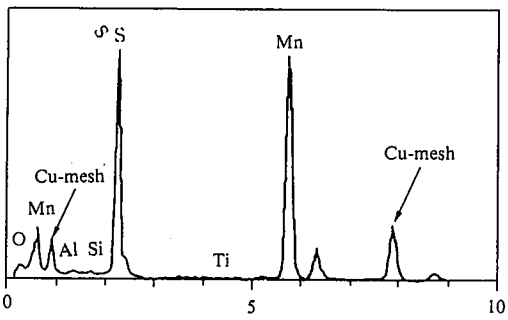

(b) Spectrum from edge of identified nonmetallic inclusions

Fig. 8 Identification results of nonmetallic inclusions in EB weld metal in low-aluminum steel

4.3.1 Test method

Titanium oxide-treated steel (L) and conventional aluminum-silicon-deoxidized steel (M), each having the chemical compositions shown in **Table 5**, were melted in a 300-ton basic oxygen furnace, continuously cast into slabs, reheated, rolled to 90-mm thick plates, and quenched and tempered. The plates were electron beam welded to a bead width of 4.5 mm and Charpy impact tested in the as-welded condition and after PWHT at 595°C for 1 h. The microstructure of the EB weld metal in the as-welded condition was observed, and the transformation nuclei of the acicular ferrite microstructure were also investigated.

4.3.2 Test results and discussion

Photo 3 shows the EB weld-metal microstructures of the titanium oxide-treated steel L and the conventional silicon-aluminum-deoxidized steel M. The steel L exhibited a microstructure primarily composed of acicular ferrite, and greatly differed from the steel M having a microstructure composed mainly of upper bainite. The EB weld-metal Charpy impact test results of the two steels are comparatively shown in **Fig. 9**. The steel L was about 30°C better in $_{v}T_{rs}$ than the steel M. **Fig. 10** shows the Charpy impact test results of the steel L in the as-welded condition and after PWHT. The impact energy was an average of 150 J in the as-welded condition and an average of about 270 J after PWHT.

Table 5 Chemical compositions of titanium oxide-treated steel L and conventional steel M

(wt%)

Symbol	C	Si	Mn	Nb	Al	Ti	N
L	0.12	0.22	1.16	0.01	0.003	0.013	0.0018
M	0.14	0.27	1.36	0.01	0.028	0.009	0.0039

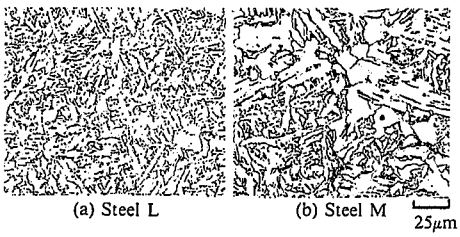

Photo 3 Comparison of microstructures of titanium oxide-treated steel L and conventional aluminum-silicon-deoxidized steel M

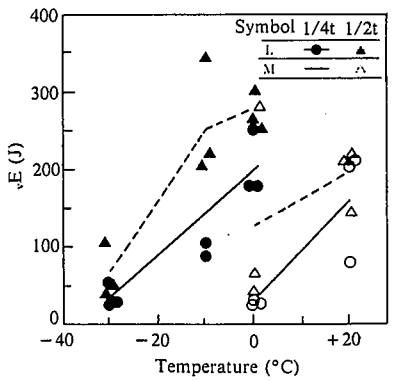

Fig. 9 Comparison of Charpy absorbed energy

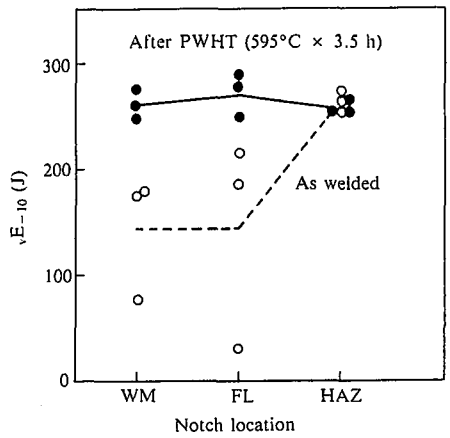

Fig. 10 Absorbed energy (1/4t) at −10°C in different notch locations of EB welded joint of steel L

Acicular ferrite transformation nuclei were chiefly composite oxides of the Al-Ti-Mn composition as shown in **Photo 4**. There were more oxide particles of less than 1 μm size in the weld metal than in the base metal, as shown in **Table 6**. This may be interpreted as suggesting that some of the oxides in the base metal were dissolved and precipitated again by EBW[20]. The steel L is comparable to the steel M in other properties and is commercialized as EB weldable steel SGV480 for pressure vessels[21].

5. Development of Quenched and Tempered Manganese-Molybdenum-Nickel Steel SQV2B for Pressure Vessels

The steel SQV2B also has compositional limitations as already described in Chapter 4. Since it has not such a low value of the ideal critical diameter Di as the steel SGV480, the steel SQV2B calls for different measures for improving the toughness of EB welds. This chapter discusses an improvement made in the toughness of EB welds in the steel SQV2B.

5.1 Analysis of factors responsible for loss of toughness

First, factors responsible for the loss of toughness of EB welds were analyzed.

5.1.1 Test method

Plates made from the conventional steel SQV2B and measuring 100 mm in thickness were electron beam welded to a bead width of 4 to 6 mm, then given PWHT at 615°C for 10 h and

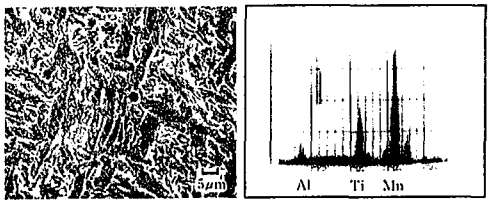

Photo 4 Nonmetallic inclusions as transformation nuclei for acicular ferrite

Table 6 Comparison of oxide size in base metal and EB weld metal

	Oxide size	
	<1.0μm	1.0-5.0μm
BM	6	21
WM	17	8

Charpy impact tested in the weld metal. The fracture condition and microstructure of the Charpy impact test specimens in the fracture initiation site and the fracture propagation site were observed.

5.1.2 Test results and discussion

(1) Observation of fracture initiation site

The fracture surface of each Charpy impact test specimen near the fracture initiation was observed under a scanning electron microscope (SEM). A typical SEM micrograph is shown in **Photo 5**. The fracture surface revealed several microcracks emanating from the fracture initiation. When the fracture surface was etched in a special etchant to observe the microcracks just below the fracture surface, the number of microcracks emanating from the fracture initiation were much greater than observed in **Photo 5**. This finding indicates that there are many microcracks not visible directly on the fracture surface.

Photo 6 shows the microstructure of the cross section just below the fracture initiation site. Microsegregation is partly connected, and microcracks are present along it. The microsegregation is believed to have formed in the solidification stage during EBW, and the microcracks are considered to have opened because of the solidification segregation of the dendrite interface.

(2) Observation of fracture propagation site

The fracture propagation site of each Charpy impact test specimen that yielded a low impact energy value was observed under the SEM. A typical SEM micrograph is shown in **Photo 7**. Intergranular cracks are observed, which is attributable to the tear-

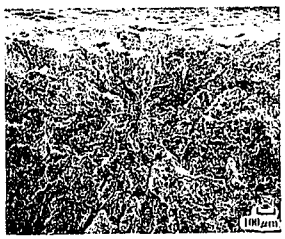

Photo 5 SEM micrograph of fracture initiation site in Charpy impact test specimen

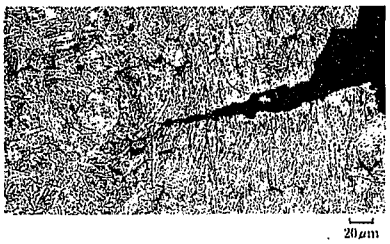

Photo 6 Microstructure of cross section just below fracture initiation in Charpy impact test specimen

Photo 7 SEM micrograph of intergranular fracture region in Charpy impact test specimen

ing off of the dendrite interface in view of their fracture morphology. The intergranular cracks are ascribable to intergranular segregation[22], which in turn is presumed to have promoted the fracture propagation.

The above discussion shows that the toughness of EB welds is reduced because: 1) the fracture initiation is a microcrack initiated along the solidification segregation; 2) the fracture propagation is promoted by intergranular cracks along the intergranular segregation; and 3) the microstructure is coarse upper bainite as described in Chapter 3.

5.2 Study of measures for improving toughness

Measures for improving the toughness of EB welds were studied on the basis of the results of the above-mentioned factor analysis.

5.2.1 Test method

The contents of alloying elements were varied by reference to the base composition of the steel SQV2B as shown in **Table 7**. The steel plates were quenched and tempered, electron beam welded with varying bead widths from 3 to 7 mm, and given PWHT at 615°C for 10 h. The microstructure of the weld metal was observed, and the fracture initiation site of Charpy impact test specimens was examined under the SEM.

5.2.2 Test results and discussion

(1) Alleviation of solidification segregation by ultralow phosphorus content

Photo 8 shows the solidification segregation of ultralow-phosphorus steel with 0.002% P and low-phosphorus steel with 0.006% P. A clear difference was observed in the solidification segregation of the dendrite interface. In the low-phosphorus steel, the solidification segregation of the dendrite interface is almost continuously connected and, additionally, the segregation zone spacing is narrow. In the ultralow-phosphorus steel, on the other hand, the solidification segregation is scattered and its spacing is wide.

For further study on the solidification segregation, a 5-mm square area at the center of each EB weld was analyzed for the segregation of phosphorus, manganese, nickel, and molybdenum by computer-aided microanalyzer (CMA). As a result, phosphorus segregation was clearly recognizable along the dendrite interface in the low-phosphorus steel, but was hardly recognizable in the ultralow-phosphorus steel. The segregation of manganese, nickel, and molybdenum was continuously connected with the dendrite interface segregation in the low-phosphorus steel, but was discontinuously connected with the dendrite interface segregation in the ultralow-phosphorus steel.

(2) Alleviation of intergranular segregation by ultralow phosphorus content

The fracture surfaces of the ultralow-phosphorus steel and low-phosphorus steel were photographed under the SEM, and their intergranular fracture surface area fractions were measured. The relationship between the intergranular fracture surface area fraction and the absorbed energy is shown in **Fig. 11**. The intergranular fracture surface area fraction is 0.7% and 0.9% for ultralow-phosphorus steel specimens with ${}_vE_{-40}$ values of 104 J and 49 J, respectively. The intergranular fracture surface area fraction is 3.4% and 3.6% for low-phosphorus steel specimens with ${}_vE_{-40}$ values of 23 J and 19 J, respectively.

The above discussion shows that the reduction in the phosphorus content to ultralow levels is considered to have alleviated the microsegregation at the dendrite interface and the microsegregation of such alloying elements as manganese, nickel and molybdenum, to have suppressed the microcracks near and just below the fracture initiation site in the Charpy impact test, and further to have reduced the intergranular fracture of the fracture propagation site, and to have improved the toughness of EB welds. It is difficult to think, however, that the intergranular fracture is a primary cause for the poor toughness of EB welds, because the maximum intergranular fracture surface area fraction is a mere 3.6%. The inhibition of microcracks by the reduction of segregation is therefore regarded as the principal contributor to improving the toughness of EB welds.

(3) Effect of other alloying elements

When the carbon content is made extremely low and alloying elements such as nickel, molybdenum and chromium are added as much as possible, the microstructural proportion of lower bainite is increased and the toughness of EB welds is improved. When the nitrogen content was lowered from the normal level of about 80 to 50 ppm, the toughness of EB welds was improved as shown in **Fig. 12**.

(4) Effect of welding conditions in optimum composition

Decreasing the bead width increases the cooling rate, increases the microstructural proportion of lower bainite, and improves the toughness of EB welds as shown in **Fig. 13**[23].

Table 7 Chemical composition ranges studied with respect to base composition of steel SQV2B

(wt%)

C	Si	Mn	P	S	Cr	Mo	Ni	Al	Ti	N
0.10	0.19	1.36	0.001	0.001	0.15	0.55	0.65	0.018	0	0.0035
↓	↓	↓	↓	↓	↓	↓	↓	↓	↓	↓
0.21	0.33	1.45	0.009	0.002	0.60	0.65	1.50	0.080	0.010	0.0096

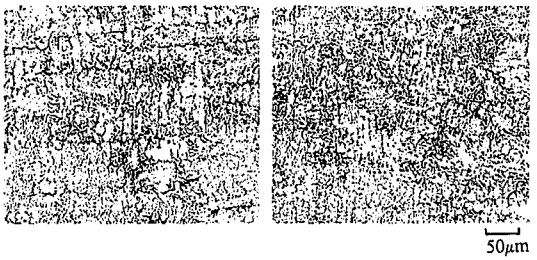

(a) Low-phosphorus steel (b) Ultralow-phosphorus steel

Photo 8 Comparison of microstructures observed at the center of EB weld metal in low-phosphorus steel (a) and ultralow-phosphorus steel (b)

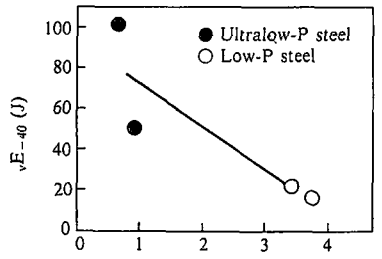

Fig. 11 Relationship between toughness and intergranular fracture surface area fraction of EB weld metal in ultralow-phosphorus steel and low-phosphorus steel

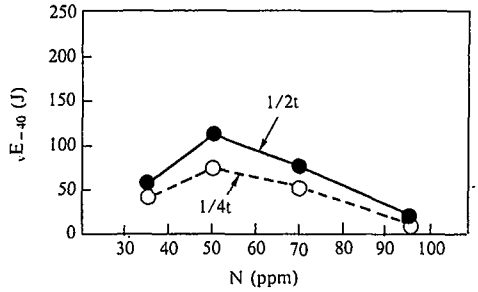

Fig. 12 Effect of nitrogen content on EB weld metal

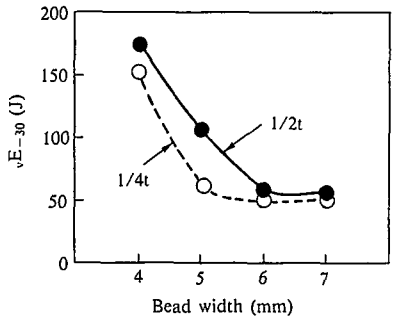

Fig. 13 Effect of bead width on EB weld metal

5.3 Properties of new steel

5.3.1 Test method

The steel SQV2B for reactor vessels with reduced contents of such contaminating elements as phosphorus and sulfur was made by the combination of basic oxygen furnace steelmaking and ladle refining, and was rolled to 100 mm thick plates. The chemical composition of the steel is as shown in **Table 8**. The plates were electron beam welded in a single pass and four passes to a bead width of 5 mm. The four-pass welding procedure simulated repair welding by cross welding technique. The welded joints were given PWHT at 615°C for 10 h.

5.3.2 Test results

Table 9 gives the Charpy impact test results of the weld metal and fusion line. The absorbed energy value was excellent at more than 200 J at the test temperature of −23°C and at more than

Table 8 Chemical composition of developed steel

(wt%)

	C	Si	Mn	P	S	Ni	Cr	Mo	Al
Developed steel SQV2B	0.18	0.26	1.43	0.002	0.002	0.67	0.15	0.57	0.027
Specifications	≦0.25	0.15	1.15			0.40		0.45	
		∣	∣			∣		∣	
		0.40	1.50			0.70		0.60	

Table 9 Charpy impact test results of EB welded joints

Number of welding passes	Test temperature (°C)	Notch location: WM, vE (J) (Average/minimum)	Notch location: FL, vE (J) (Average/minimum)
1	−23	270/261	238/214
	−40	248/241	236/197
	−50	256/240	187/180
4	−23	221/217	278/271
	−40	162/152	238/205
	−50	123/105	188/160

Table 10 NLR drop weight test results

Number of welding passes	Notch location, T_{NDT} (°C)	
	WM	HAZ
1	−60	−60
4	−55	−70

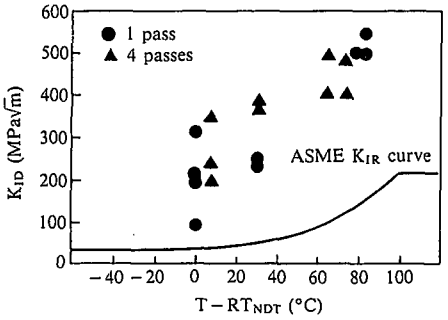

Fig. 14 Dynamic fracture toughness test results of EB welded joints

Table 11 Weld metal toughness comparison of various welding processes

Welding process	WM toughness $_vE_{-23}$ (average/minimum)
EBW	270/261
SAW	151/123
Narrow-gap SAW	230/173
Narrow-gap GMAW	153/142

100 J at the test temperatures of −40°C and −50°C, irrespective of whether or not the EB weld was made in a single pass or four passes. **Table 10** shows the drop weight test results for specimens with the notch machined in the weld metal or HAZ. Each specimen exhibited a good nil-ductility temperature (T_{NDT}) of −55°C or less. Excellent dynamic fracture toughness test results were also yielded as shown in **Fig. 14**[24].

5.3.3 Comparison of EBW with conventional welding processes

The welding test results of the steel SQV2B by EBW are compared with those by other welding processes as shown in **Table 11**[25]. EBW provided weld metal toughness equal to or better than that provided by the conventional welding processes. The steel SQV2B has a carbon equivalent (Ceq) of as high as 0.63%, which would otherwise complicate preheating temperature control for the conventional welding processes. EBW improves not only the welding efficiency, but also the weld metal properties.

The newly developed steel is not inferior to conventional steels also in other properties and is commercially used as electron beam weldable steel SQV2B for pressure vessels[26].

6. Conclusions

Electron beam welding (EBW) is expected to enhance the welding efficiency of heavy steel plates for pressure vessels and in similar applications. The problem of blowholes was solved by beam oscillation and other advanced EBW techniques. The last remaining problem was improving the weld toughness by investigating the use of conventional steels. On the basis of the results obtained, measures were taken to improve the toughness of EB welds. The following findings were derived:

(1) When the toughness of EB welded joints of conventional steels was investigated, EB welded joints of 490-MPa and 590-MPa

steels exhibited a coarse upper bainite microstructure and were low in toughness.

(2) When the toughness of EB welded joints in the as-welded condition and after PWHT was investigated by systematically varying the chemical composition and bead width, centering on the 490-MPa steels, the ${}_{v}T_{r}$ (70 J) = 0°C line was successfully arranged by the carbon content and the ideal critical diameter Di.

(3) Controlling the aluminum/oxygen content ratio was found to yield a microstructure consisting predominantly of acicular ferrite in order to improve the EB weld metal toughness of the 490-MPa steels. On the basis of this finding, a low-aluminum, titanium-oxide steel, designated SGV480, was developed for pressure vessels and similar electron beam weldable structures.

(4) Reducing the phosphorus content to an extremely low level and thereby alleviating the solidification segregation of the electron beam weld metal and reducing microcracks at the fracture initiation site were found to improve the toughness of the electron beam weld metal of the 590 MPa steel. This finding led to the development of the ultralow-phosphorus, low-nitrogen and low-carbon steel designated SQV2B.

References

1) Onoue, H.: Journal of the Japan Welding Society. 54 (2), 102 (1985)
2) Shono, S. et al.: Proc. of 6th Int. Conf. on Pressure Vessel Technology, Beijing, September 1988, 2, p. 1297
3) Sakabata, N. et al.: Quarterly Journal of the Japan Welding Society. 4 (1), 131 (1986)
4) Shida, T. et al.: Journal of the Japan Welding Society. 48 (10), 813 (1979), and other references
5) Nakanishi, M. et al.: Sumitomo Metal. 33 (2), 169 (1981)
6) Uratani, Y. et al.: Mitsubishi Heavy Industries Technical Review. 24 (1), 30 (1987)
7) Arata, Y. et al.: Journal of the Japan Welding Society. 44 (12), 1011 (1975)
8) Kosuge, S. et al.: Quarterly Journal of the Japan Welding Society. 3 (2), 291 (1985)
9) Ohara, M. et al.: Report presented at 51st meeting of Electron Beam Research Committee. EBW-398-87, 1987
10) Seo, K. et al.: Journal of the Japan Welding Society. 51 (3), 291 (1982)
11) Kanaya, K. et al.: Tetsu-to-Hagané. 71 (5), 306 (1985)
12) Ohara, M. et al.: IIW Doc. IX-1674-92, Madrid, September 1992
13) Ohkita, S. et al.: Proc. of Joint Australian Welding & Testing Conf. Perth, October 1984
14) Ohara, M. et al.: Proc. of Int. Conf. on Electron and Laser Beam Welding. Tokyo, July 1986
15) Devillers, L. et al.: Proc. Int. Conf. the Effect of Residual, Impurity and Microalloying Elements on Weldability and Weld Properties, Paper 1, London, November 1983
16) Ohara, M. et al.: Int. Conf. on Application of Electron and Laser Beam Welding. Hartford, September 1987
17) Ohara, M. et al.: 4th Int. Colloq. on Welding and Melting by Electron and Laser Beam. Canne, September 1988
18) Ohara, M. et al.: CAMP-ISIJ. 1 (3), 908 (1988)
19) Yamamoto, K. et al.: Symp. on Residual and Unspecified Elements in Steel. Florida, November 1987
20) Chijiiwa, R. et al.: CAMP-ISIJ. 1 (3), 909 (1988)
21) Matsumoto, O. et al.: 4th Int. Colloq. on Welding and Melting by Electron and Laser Beam. Canne, September 1988
22) Ouchi, C. et al.: Toward Improved Ductility and Toughness. Kyoto, October 1971, p. 67
23) Koyama, K. et al.: Proc. of PACRIM WELDING '92. Paper 15, Darwin, June 1992
24) Tomita, Y. et al.: ASME Pressure Vessels and Piping Conf. New Orleans, June 1992
25) Kikutake, T. et al.: Boiler and Nuclear Power. 33 (6), 509 (1982)
26) Takano, G. et al.: Pre-prints of the National Meeting of JWS. 49, 1991, p. 278